A THEORETICAL ANALYSIS OF THE DECOMPOSITION KINETICS OF SUPERSATURATED SOLID SOLUTIONS

L. N. ALEKSANDROV and B. Ya. LYUBOV

Usp. Fiz. Nauk 75, 117-150 (September, 1961)

I. INTRODUCTION

IT is extremely important to study the kinetics of the decomposition of supersaturated solid solutions for both theoretical and practical reasons. Investigations in this branch of the science of metals and alloys determine the factors that affect processes taking place during heat treatment, and thus determine the possibilities of different metastable states. The methods used in the theoretical analysis of these processes are based on the thermodynamics of nonequilibrium states and the laws of physical kinetics; therefore this field of study is also of interest from a general physical point of view.

Both physical kinetics and the thermodynamics of nonequilibrium states are subjects of comparatively recent development. Difficulties are encountered in applying these branches of theoretical physics to the solution of specific problems. Moreover, the existing theory of phase transformations was developed with reference to vapor condensation processes. Great care must be exercised in applying this theory to the analysis of crystallization from the liquid state, and even more so in examining the characteristics of transformations in solid metals and alloys. Because of this situation relatively few investigations have been made of the kinetics of solid-state phase transformations. Among the basic problems awaiting solution are the effects of stresses arising during phase transformations and the effect that anisotropy of the medium has on the rate of nucleation and the form of a new phase. In the present investigation we do not consider the crystalline properties of the medium undergoing a phase transformation. This is obviously permissible at sufficient high temperatures.

We shall confine our analysis to the kinetics of the decomposition of supersaturated solid solutions. Because of the great complexity of the processes involved and the large number of factors affecting them in each individual problem, our scheme of calculation will consider only the principal characteristics of the phenomena in question. In the decomposition of a supersaturated binary solid solution the new phase can differ from the original phase with regard to the original lattice type or composition, or both simultaneously. Therefore in the general case the diffusional redistribution of solute atoms will be accompanied by transitions of the solvent from one modification to another or by the formation of a new chemical compound. The first of these processes is associated with the movement of atoms through distances considerably greater than atomic separations, while the second process amounts to a reorganization of the solvent lattice at the phase interface. In our investigation we assume that the isothermal decomposition rate of a supersaturated solid solution is determined by the kinetics of that particular process, among the simple processes required for the transformation, which produces the smallest amount of the new phase in a given time interval and plays the part of a limiting factor in the transformation. In the case of a ternary system the retarding factor can be the diffusion of the third element. We shall show that the introduction of the latter can in some instances change the retardation factor of the process. Our theoretical analysis will be illustrated with examples pertaining to processes occurring during the heat treatment of both plain carbon and alloy steels. The results can clearly be used for the study of similar processes occurring in other metallic systems.

We shall consider successively the kinetics of phase transformations in one-component, binary, and ternary systems. Pertinent experimental investigations have been performed by the groups of G. V. Kurdyumov,[1] S. S. Shteĭnberg,[2] and S. T. Konobeevskii.

II. ONE-COMPONENT SYSTEMS

In a one-component system, such as a polymorphic metal, cooled below the stability range of the high-temperature phase, regions appear in which the structure of a new modification is exhibited. Under the influence of thermodynamic factors these regions, if they exceed a certain critical size, grow until they occupy the entire volume of the system.[3] (Regions of less than critical size will be called embryos, and larger regions will be called nuclei (or centers), of the new phase.) Thus the nuclei of the new phase grow steadily while embryos shrink and tend to disappear. However, in any system fluctuations occur consisting in local departures of the system from equilibrium in the direction opposite to that expected thermodynamically. The existence of fluctuations enables the embryos to increase to a size suitable for stable growth. Since the number of small embryos exceeds the number of large embryos, their enlargement as a result of fluctuations is more probable than the reverse. Therefore the growth of embryos results

from the systematic influence of thermodynamic forces and from fluctuation-induced size changes. At each moment during an isothermal period t of a system its metastable phase is described by the distribution Z (g, t) of regions of the new modification with respect to the contained number of atoms:[4,5]

$$\frac{\partial Z(g,t)}{\partial t}=\frac{\partial}{\partial g}\left[D(g)\,b(g)\,\frac{\partial}{\partial g}\frac{Z(g,t)}{b(g)}\right], \tag{1}$$

where D (g) is the probability that an embryo containing g atoms will acquire an additional atom in unit time, and b (g) is the equilibrium size distribution of embryos at which detailed balancing is established in the system. b (g) is determined from

$$b(g)=Ne^{-\frac{\Delta\Phi(g)}{kT}},$$

where N is the total number of atoms in the system, and $\Delta\Phi(g)$ is the change in the thermodynamic potential of the system when an embryo consisting of g atoms is formed.[6] The solution of Eq. (1) under the conditions conventionally assumed in studying phase transformations after a nonsteady-state period,[7] enables us to determine the nucleation rate of new-phase centers, i.e., the number of embryos transformed into nuclei per unit time per unit volume of the metastable state is

$$I=\text{const}\cdot\exp\left(-\frac{u}{kT}\right)\exp\left(-\frac{w}{kT}\right), \tag{2}$$

or, as follows from reference 8,

$$I=\frac{\alpha}{v_0}\left(\frac{RT}{h}\right)\exp\left(-\frac{u}{kT}\right)\exp\left(-\frac{w}{kT}\right), \tag{3}$$

where

$$w=\frac{1}{3}\sigma S_{cr},\quad S_{cr}=4\pi\varrho_{cr}^2,\quad \varrho_{cr}=\frac{2\sigma}{\Delta F_0},$$

σ is the surface tension at the phase boundary, ΔF_0 is the change in free energy accompanying the formation of a unit volume of the new phase, ρ_{cr} is the critical nuclear radius, h is Planck's constant, R is the gas constant, v_0 is the specific volume, α is determined by the structure and varies from 1 to 10 ($\alpha/v_0 \approx 1$ cm^3/mole), and u is the activation energy for the transfer of atoms through the phase interface.

The description of the phase transformation process requires knowledge of the rate of directed growth as well as the nucleation rate. For a spherical center[9,10] of radius ρ, assuming the average frequency of atomic vibrations at the phase interface to be $\omega = \omega_{max} = k\theta_D/h$, (where θ_D is the Debye temperature), and also assuming* $T = \theta_D$, we obtain

$$v=\frac{d\varrho}{dt}=\frac{16\pi r_a^4\Delta F_0}{9h}\left(1-\frac{\varrho_{cr}}{\varrho}\right)\exp\left(-\frac{u}{kT}\right), \tag{4}$$

where r_a is the atomic radius. Equation (4) is valid when[10]

$$\left|\frac{\Delta F_0}{2RT}\left(1-\frac{\varrho_{cr}}{\varrho}\right)\right|\ll 1. \tag{5}$$

When $\rho \to \infty$ we have

$$\frac{d\varrho}{dt}=\frac{16\pi r_a^4\Delta F_0}{9h}\exp\left(-\frac{u}{kT}\right). \tag{6}$$

Since the volume of a single atom is given by

$$\frac{4}{3}\pi r_a^3=\frac{v_0}{N},$$

for a flat interface we have

$$\frac{dx}{dt}=\frac{\Delta F_0}{\pi h r_a^2}\left(\frac{v_0}{N}\right)^2\exp\left(-\frac{u}{kT}\right), \tag{7}$$

where x is the boundary coordinate. In experimental investigations of the kinetics of isothermal transformations in one-component systems, as in other phase transformations, it is customary to determine the kinetic curve, which is the dependence of the new-phase volume V on the isothermal period t. If the nucleation rate I and the growth rate $d\rho/dt$ are known as functions of t and temperature, the analytical determination of V (t) is a purely mathematical problem, which has been solved by A. N. Kolmogorov under certain assumptions in reference 11.

For the kinetic curve of the isothermal process we have

$$\frac{V(t)}{V_0}=1-\exp\left[-\int_0^t I(\tau)\,f(t-\tau)\,d\tau\right], \tag{8}$$

where V_0 is the initial volume and f (t) is the volume of the new-phase center at time t. Assuming steady creation of centers and confining ourselves to sufficiently large ρ, we transform to the molar quantities U = Nu and W = Nw, where N is Avogadro's number, and from (3) and (6) we obtain

$$\frac{V(t)}{V_0}=\eta=1-\exp\left[-\frac{\pi^4 d^{12}(\Delta F_0)^3 RT}{3^7 h^4}\exp\left(-\frac{W+4U}{RT}\right)t^4\right]. \tag{9}$$

Here $d = 2r_a$ and η is the transformed fraction of the initial volume. From (9) we obtain the transformation time for the fraction η of the volume:

$$t_\eta=\frac{3h}{8\pi r_a^3\Delta F_0}\left[-\frac{27\ln(1-\eta)\,\Delta F_0\cdot\alpha}{RTv_0}\right]^{1/4}\exp\left(\frac{\frac{1}{4}W+U}{RT}\right). \tag{10}$$

Thus with η given, Eq. (10) furnishes t as a function of T.

III. BINARY SYSTEMS

1. Growth Rate of a Nucleus of a New Phase in the Decomposition of a Supersaturated Noneutectoid Solid Solution

The phase transformation involved in the decomposition of a supersaturated binary solid solution cannot be attributed, as was done for one-component solutions, solely to lattice reconstruction at the interphase boundary. The difference between the composition of the initial solid solution and that of the new phase shows that

*These assumptions simplify the calculations without changing essentially the computed result for the growth rate of a center.

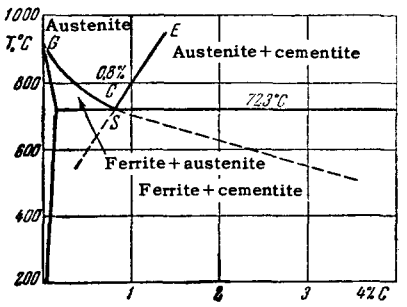

FIG. 1. A portion of the Fe-C constitution diagram.

the process requires diffusional redistribution of the dissolved component in addition to a change of the solvent lattice.

It is usually assumed that the growth rate of new-phase centers is determined by the diffusion rate of the solute. This assumption has been used by Pines,[12,13] Zener,[14,15] and others. However, it is sometimes possible that reorganization of the solvent lattice is the controlling process. As an example we shall consider the decomposition of austenitic steel, an interstitial solid solution of carbon in the high-temperature modification γ-Fe which has a face-centered cubic lattice.[16] A similar solution of carbon in low-temperature body-centered α-Fe is called ferrite. The equilibrium carbon content in austenite does not exceed 1.7%; carbon exhibits very low solubility in α-Fe.[17] An important structural component of steel is cementite (Fe_3C), which has a rhombohedral lattice containing 6.67% carbon. The iron-carbon constitution diagram in Fig. 1 shows the stability regions of different phases of steel. The austenite stability region is bounded by the lines GS and SE. In connection with heat treatment it is important to study the decomposition of undercooled austenite at temperatures below 723° C.[18] The structure and composition of the phases resulting from the isothermal decomposition of austenite depend essentially on the original composition and the degree of undercooling. We shall limit our discussion to the growth rate of new-phase nuclei in isothermal austenite decomposition within the upper region of subcritical temperatures (723 — 500° C).

Since we are interested in determining the physical mechanism of the investigated effects, we shall study the initial stage of the transformation during which nuclei grow practically independently. Later stages begin to be affected by such factors as contact between nuclei, altered solid-solution concentration as a result of decomposition[19,20] etc. The iron-carbon diagram exhibits a eutectoid point S at 723° C for 0.8% carbon content (Fig. 1). Undercooled eutectoid austenite maintained isothermally in the upper range of subcritical temperatures decomposes into alternate plates of ferrite and cementite, forming a distinctive structure called pearlite. If the austenite has under 0.8% carbon initially the decomposition begins with the formation of ferrite nuclei in the undercooled

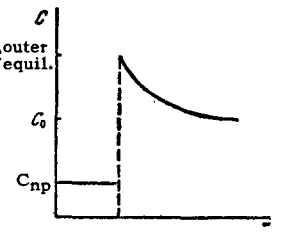

FIG. 2 Distribution of concentrations ahead of the front of a growing grain for $C_0 < C_\infty$.

phase; these nuclei grow in a nearly spherical shape. As the quantity of ferrite increases the carbon concentration in the remaining autenite is enhanced, approaching the eutectoid point. When the latter is reached the pearlite transformation takes place. Thus the decomposition of hypoeutectoid austenite results in a structure consisting of ferrite grains surrounded by pearlite. Similarly, the decomposition of hypereutectoid austenite produces carbide grains in a pearlite matrix.

Let us consider the growth of a ferrite nucleus in undercooled hypoeutectoid austentite. If during growth the outer side of the nuclear surface is in a region with the equilibrium concentration[13]

$$C_\varrho = C_\infty^f e^{v_c \frac{2\sigma}{RT\varrho}} \cong C_\infty^f \left(1 + v_c \frac{2\sigma}{RT\varrho}\right) \qquad (11)$$

(where C_∞ is the solute concentration in the old phase when the two phases separated by a plane are in equilibrium and v_c is the atomic volume of the solute), the rate of the process is determined by the carbon diffusion rate.

It should be noted that (11) is not firmly established. It is necessary to investigate further the equilibrium conditions for coexisting phases taking into account the thermodynamics of solid solutions.[21] For small nuclei we assume that the concentration distribution of the solute, given spherical symmetry, is represented by

$$\Delta C = \frac{\partial^2 C}{\partial r^2} + \frac{2}{r}\frac{\partial C}{\partial r} = 0. \qquad (12)$$

The carbon concentration decreases with distance from the nuclear surface, approaching the original value C_0 (Fig. 2). The concentration inside of the nucleus has the equilibrium value C_{np} for the given temperature. It is clear that

$$(C_0 - C_{np})\frac{4}{3}\pi\varrho^3 = 4\pi\int_\varrho^\infty [C(\varrho, t) - C_0]\varrho^2 d\varrho. \qquad (13)$$

It can be shown that in the case of a nonsteady-state concentration distribution represented by

$$\Delta C = \frac{1}{D}\frac{\partial C}{\partial t} \qquad (14)$$

(where $D = D_0 e^{-Q/RT}$ is the diffusion coefficient, D_0 is the coefficient of the exponential, and Q is the activation energy for diffusion), Eq. (13) assumes the differential form

$$(C_\varrho - C_{np})\frac{d\varrho}{dt} = -D\left(\frac{\partial C}{\partial r}\right)_{r=\varrho}. \qquad (15)$$

For a steady state Eq. (15) is a valid approximation

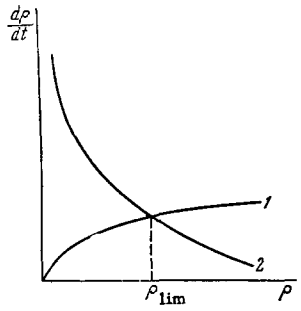

FIG. 3. Growth rate of a ferrite grain determined by (1) the kinetics of lattice reconstruction, and (2) carbon diffusion.

for small ρ and low supersaturation.

In our case the solution of (12) becomes

$$C(r, t) = (C_\varrho - C_0)\frac{\varrho}{r} + C_0. \quad (16)$$

Substituting (16) in (15), we obtain

$$\frac{d\varrho}{dt} = D\frac{C_\varrho - C_0}{C_\varrho - C_{np}}\frac{1}{\varrho}. \quad (17)$$

According to (11) the new-phase nucleus should have a very rapid growth rate for small ρ. On the other hand, the growth of a ferrite nucleus of near-critical size is marked by relatively slow change of the solvent (iron) structure, since the thermodynamic advantage of reconstruction of the iron lattice in this range of nuclear dimensions is very insignificant. During the growth of a nucleus, excess carbon is precipitated from the volume occupied by the new phase and appears on the nuclear surface. Because of the small nuclear size the carbon deposited on its surface produces almost no change in the solute concentration in that region. It can therefore be assumed that during the first growth stage the solute concentration on the nuclear surface has practically the initial value C_0. On the other hand, if Eq. (11) is applicable the equilibrium concentration for these nuclei is relatively large. Thus the true concentration on the surface of a small nucleus is below the equilibrium value. In this stage of growth carbon can be accumulated on the nuclear surface and the process rate is determined by the kinetics of reconstruction of the solvent lattice. As the nucleus grows its growth rate is accelerated and the concentration outside of the phase boundary approximates C_ρ. Finally, the nuclear radius approaches a limit ρ_{lim} when the concentration on the nuclear surface is C_ρ. The retarding effect of the solute diffusion rate now becomes important and the process rate is determined by diffusion.[9,22] In actuality there is no sharp demarcation between different periods in the growth of a nucleus. The transition from one growth mechanism to another is gradual and cannot be associated with any precise size.* It follows from the described scheme that the growth of new-phase regions from the minimum size at which we are entitled to speak of a definite structure up to the limiting radius ρ_{lim} is described by Eq. (4). ρ_{lim} corresponds to the equivalence of (4) and (17) (Fig. 3). In the latter equation we shall assume for simplicity $C_\rho = C_\infty$, which is valid if $v_c(2\sigma/RT\rho_{lim}) \ll 1$. In this approximation we obtain

$$\varrho_{cr} = \frac{27D_0h}{16\pi r_a^4 \Delta F_0}\frac{C_\infty - C_{np}}{C_0 - C_{np}}\exp\left(\frac{U-Q}{RT}\right) + \frac{2\sigma}{\Delta F_0}. \quad (18)$$

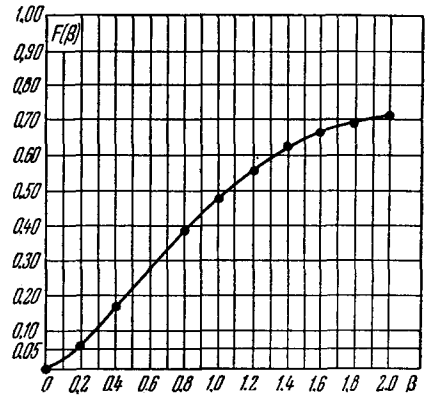

FIG. 4. Graph of the function $F(\beta)$.

The foregoing discussion can be applied to the precipitation of cementite from undercooled hypoeutectoid austenite, keeping in mind that ρ_{lim} can theoretically also be smaller than ρ_{cr}, i.e., a nuclear radius corresponding to the limiting role of the lattice reconstruction mechanism is possible but not required.

When $\rho \to \infty$ we have $C_\rho \to C_\infty$. The condition for the surface of a nucleus then becomes

$$C[\varrho(t), t] = C_\infty. \quad (19)$$

Moreover,

$$C(\infty, t) = C_0. \quad (20)$$

In this case the mathematical difficulty of the solution is considerably alleviated and it becomes possible to solve the nonsteady-state diffusion equation (14), for which (15) is an exact condition.[23,24] We obtain

$$C(r, t) = C_0 + (C_\infty - C_0)\frac{\frac{2\sqrt{Dt}}{r}e^{-\frac{r^2}{4Dt}} - \sqrt{\pi}\,\mathrm{erfc}\left(\frac{r}{2\sqrt{Dt}}\right)}{\frac{1}{\beta}e^{-\beta^2} - \sqrt{\pi}\,\mathrm{erfc}\,\beta}, \quad (21)$$

where

$$\mathrm{erfc}\,\beta = \frac{2}{\sqrt{\pi}}\int_\beta^\infty e^{-\xi^2}d\xi = 1 - \mathrm{erf}\,\beta.$$

Substituting (21) in (15), we obtain

$$\varrho(t) = 2\beta\sqrt{Dt}, \quad (22)$$

where β is a root of the transcendental equation

$$\frac{C_\infty - C_0}{C_\infty - C_{np}} = 2\beta^2(1 - \beta\sqrt{\pi}e^{\beta^2}\mathrm{erfc}\,\beta) = F(\beta). \quad (23)$$

The function $F(\beta)$ is represented by Fig. 4. It follows directly from (22) that

*B. Ya. Pines has considered the growth of a new-phase nucleus during a steady-state stage of phase transformation in a substitutional solid solution.[65]

$$v=\frac{d\varrho}{dt}=\frac{\beta\sqrt{D}}{\sqrt{t}}=\frac{2\beta^2 D}{\varrho}. \quad (24)$$

During the growth of a ferrite grain C_∞^f is determined by extrapolating the GS curve of the iron-carbon phase diagram (Fig. 1). The analytical expression for this quantity is

$$C_\infty^f=0.8+0.013(996-T). \quad (25)$$

We shall consider the case $C_0 = 0.5\%$ and $C_{np} = 0.04\%$. At T = 993° Eq. (25) gives $C_\infty^f = 0.839\%$. Thus $F(\beta) = 0.4$, and from Fig. 4 we have $\beta \cong 0.8$. The carbon diffusion coefficient in austenite depends on temperature and the carbon concentration as follows:[25]

$$D(C)=(0.04+0.08\%\,C)e^{-\frac{31350}{RT}}\ \text{cm}^2/\text{sec} \quad (26)$$

The carbon concentration in the region surrounding a ferrite grain varies from C_∞^f to C_0. We take the average of D in this range of concentrations:

$$\overline{D(C)}=\frac{1}{C_\infty^f-C_0}\int_{C_0}^{C_\infty^f} D(C)\,dC$$

$$=0{,}04(1+C_0+C_\infty^f)e^{-\frac{31\,350}{RT}}\ \text{cm}^2/\text{sec}. \quad (27)$$

Substituting the value obtained for β and the corresponding value of $\overline{D(C)}$ in (24), we obtain

$$v=\frac{9.4}{\sqrt{t}}10^{-4}\ \text{mm/sec}. \quad (28)$$

The experimental growth rate[26] of a ferrite grain is compared with Eq. (28) in Fig. 5. It is important to note in connection with our subsequent discussion that the calculated curve, although lying below the experimental curve, gives a good representation of the way in which the isothermal growth rate of a ferrite nucleus varies with time.

The considerations leading one of the present authors to Eq. (24), which were presented in reference 23 at the beginning of 1948, were also published by Zener at the end of 1949.[14] Zener did not mention reference 23 and stated that he knew no solution of the foregoing problem for the spherically symmetrical case.

The dependence of the isothermal growth rate of a ferrite nucleus on the temperature at which austenite decomposes is given by the factor $\beta\sqrt{D(C)}$, which is a function of C_0 and T. Figure 6 shows $\beta\sqrt{D(C)}$ as a function of T for different values of C_0. The solid curve in the figure connects the maximum growth

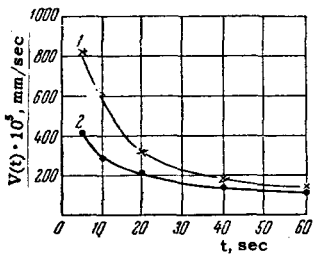

FIG. 5. Growth rate of a ferrite grain at 720°C. Curve 1 – experimental; curve 2 – calculated.

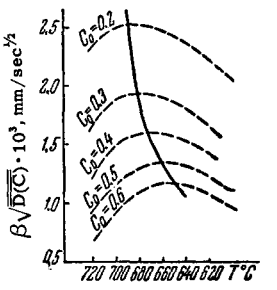

FIG. 6. Growth rate of a spherical ferrite nucleus $\beta\sqrt{D(C)}$ vs T and the initial carbon concentration C_0.

rates at different initial carbon concentrations. This figure agrees qualitatively with the growth rate of a nucleus as a function of the initial concentration and of temperature that was obtained by A. A. Bochvar in an experimental investigation of the crystallization of eutectic alloys.[27]

For a spherical cementite nucleus, taking $C_0 = 1.2\%$ and T = 993° and considering that cementite-austenite equilibrium is subject to the condition

$$C_\infty^c=0.8-0.002(996-T), \quad (29)$$

we find $F(\beta) = 0.07$, $\beta = 0.2$, and

$$v=\frac{2.4}{\sqrt{t}}10^{-4}\ \text{mm/sec}. \quad (30)$$

Figure 7 shows the dependence of the growth rate of a cementite nucleus ($\beta\sqrt{D(C)}$, t = 1 sec) on T and the initial carbon concentration.[28]

During the annealing of steel, carbide plates with rounded edges are apparently precipitated.[29] If the thickness-length ratio of a plate is small its edge can be approximated by a parabolic cylinder.[30] In Fig. 8 the y axis is perpendicular to the x axis lying in the horizontal cross section of a plate. The solute distribution ahead of the edge of a growing plate is given by

$$\frac{\partial C}{\partial t}=D\left(\frac{\partial^2 C}{\partial x^2}+\frac{\partial^2 C}{\partial y^2}\right). \quad (31)$$

The differential form of the mass balance equation is

$$(C_{np}-C_\infty^c)\frac{d\bar{n}}{dt}=-D\left(\frac{\partial C}{\partial \bar{n}}\right)_{u=1}, \quad (32)$$

where $\bar{n}$ is the normal to the interface and u is a dimensionless variable defined as the ratio of the radius of curvature ρ at the vertex of the parabola through a given point to the radius of curvature ρ_0 at the vertex of the parabola representing the interface

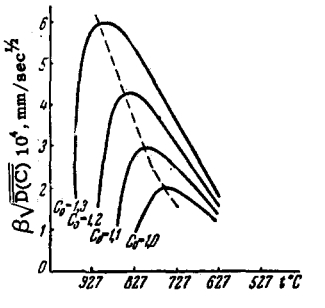

FIG. 7. Growth rate of a spherical cementite nucleus $\beta\sqrt{D(C)}$ vs T and the initial carbon concentration C_0.

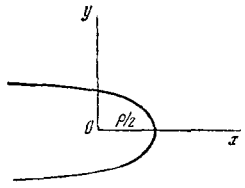

FIG. 8. Schematic drawing of the edge of a growing new-phase plate at t = 0.

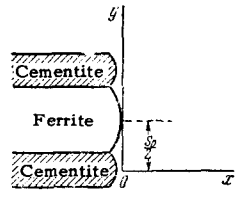

FIG. 10. Schematic outline of the edge of a pearlite grain.

(in two dimensions). Assuming that a steady state is rapidly established at the interface, the growth rate v of a cementite plate is not time-dependent. C is a function of the complicated argument

$$u=\frac{\varrho}{\varrho_0}=\frac{1}{\varrho_0}\left(x-vt+\sqrt{(x-vt)^2+y^2}\right). \qquad (33)$$

Solving the diffusion equation (31) subject to the conditions

$$C(\infty)=C_0, \qquad C(1)=C^c_\infty, \qquad (34)$$

we obtain

$$C(u)=C_0+(C^c_\infty-C_0)\frac{1-\operatorname{erf}\sqrt{\frac{pu}{2}}}{1-\operatorname{erf}\sqrt{\frac{p}{2}}}, \qquad (35)$$

where

$$p=\frac{v\varrho_0}{D}.$$

Substituting (35) in (32), we obtain a transcendental equation for p:

$$\varphi(p)=\sqrt{\frac{\pi p}{2}}e^{\frac{p}{2}}\operatorname{erfc}\sqrt{\frac{p}{2}}=\frac{C^c_\infty-C_0}{C^c_\infty-C_{\text{np}}}. \qquad (36)$$

This function is shown in Fig. 9.

As an example let us consider the growth of carbide platelets at T = 993° and C_0 = 1.2%. p = 0.005 is obtained. The maximum growth rate of a platelet corresponds to $\rho_0 \cong 2\rho_{cr}$ and is calculated to be 0.4×10^{-3} mm/sec.

2. The Growth Rate of a New Phase in the Decomposition of a Eutectoid Solid Solution

Pearlite results from the decomposition of undercooled eutectoid austenite, as already stated. At the present time the mechanism responsible for the formation of the lamellar structure of pearlite is not clearly understood. Insufficient data are available for a quantitative analysis of the pearlite nucleation rate. We shall outline a hypothetical qualitative model of pearlite nucleation. It is assumed that the transformation begins with the appearance of a carbide nucleus in undercooled eutectic austenite. As this nucleus grows, the carbon content diminishes in the austenite region adjacent to the surface of the nucleus; therefore the probability of the creation of a ferrite nucleus increases. A ferrite nucleus arising adjacent to a cementite center precipitates carbon. There is now relatively less carbon at the side of the cementite nucleus opposite the first ferrite nucleus. The most favorable conditions are thus created for a second ferrite nucleus, so that ferrite nuclei now border the cementite nucleus on both sides. Growth ceases in the contact regions between the nuclei. Similarly, a new cementite nucleus should arise adjacent to each ferrite nucleus, leading to a chain of alternating cementite and ferrite nuclei. In time the links of the chain, which were originally spherical, will flatten out because growth ceases at the surfaces in contact. The ultimate pearlite nucleus consists of alternate ferrite and cementite layers (Fig. 10). This qualitative discussion will now be confirmed by quantitative estimates.

Let us consider a cementite lamella with equilibrium carbon concentration at its surface, varying from point to point in accordance with the changing radius of curvature of the interface. The radius of a critical ferrite nucleus should depend, from a rigorous point of view, on the carbon concentration in the initial and final phases, although the formation mechanism amounts to reordering of the solvent lattice. This follows from the fact that ΔF_0 varies with C_0 and C_{np}; this has been taken into account as proposed in reference 31. Taking σ = 70 erg/cm^2, T = 873°, and U = 35 kcal/mole, and

$$\Delta F_0=N_{\text{Fe}}\Delta F^{\gamma\to\alpha}_{\text{Fe}}+N_{\text{C}}(10\,500-3.425T)+\Delta F_* \qquad (37)$$

(where N_{Fe} and N_C are the mole fractions of iron and carbon, and ΔF_* is associated with the ordering of the solid solution and is negligibly small in our present case), we obtain the result depicted in Fig. 11. The probability of the appearance of a ferrite nucleus at a plane austenite-cementite interface is much greater than at the edge of a cementite plate.

Thus a pearlite nucleus grows both by the joining of new ferrite and cementite nuclei, and by the ad-

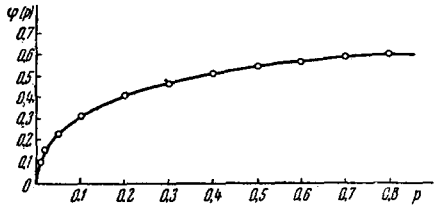

FIG. 9. Graph of φ(p).

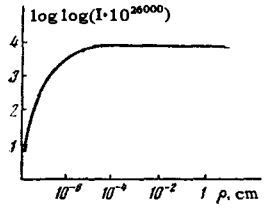

FIG. 11. Ferrite nucleation rate at austenite-cementite interface vs. curvature of the interface.

vance of the edges of ferrite and cementite lamellae into undercooled austenite.[31] As in the case of single-phase precipitation, the growth of eutectoid grains can be limited either by the kinetics of lattice reconstruction or by the carbon diffusion rate in austenite.

We shall confine ourselves here to the second of these possible processes. We shall calculate the edgewise growth rate of a pearlite grain, which means the rate of advance of the edges of ferrite and cementite lamellae in the pearlite transformation. When the growth rate of a pearlite nucleus is determined experimentally we obtain an average value depending on the edgewise growth rate of the pearlite nucleus and the creation rate of ferrite and cementite nuclei in the direction perpendicular to the contact plane between ferrite and cementite lamellae. Since pearlite grains are almost spherical we can expect close agreement between the experimental rate and the calculated edgewise growth rate of these grains.

The actual calculation requires the determination of the carbon concentration at a pearlite grain surface. In our foregoing discussion of the new-phase growth rate at noneutectoid concentrations we showed that after a transition through a definite limiting size an equilibrium concentration, depending on the decomposition temperature and nuclear radius, is established outside of the nuclear surface and is maintained during subsequent growth. In the case of pearlite we have at a cylindrical cementite-austenite interface

$$C_Q^c = C_\infty^c e^{v_c \frac{\sigma_{ac}}{RTQ_c}}, \tag{38}$$

and at a ferrite-austenite interface

$$C_Q^f = C_\infty^f e^{v_c \frac{\sigma_{af}}{RTQ_f}}, \tag{39}$$

where σ_{ac} and σ_{af} are the surface tensions on the respective phase boundaries.

Before proceeding with the proposed method of calculating the edgewise growth rate of pearlite centers, we shall discuss reference 32, which is concerned with the same problem. On the basis of experimental data Brandt assumes that the edges of the ferrite and cementite lamellae in pearlite advance at a constant rate into the original austenite, and writes the diffusion equation describing the redistribution of carbon in austenite in a moving coordinate system with its origin at the center of the edge of a cementite lamella. The diffusion equation will thus be solved in a coordinate system moving at constant velocity along the abscissal axis, for a region bounded on one side by a complex curve (the pearlite-austenite boundary) of unknown shape. Unjustifiable simplifications are introduced because of the complexity of this formulation. The function describing the carbon concentration in austenite is written as an infinite series cut off at the third term; the coefficients of all higher terms are thus assumed to vanish. Supplementary conditions are used to determine the coefficients of the first three terms.

According to a general theorem of mathematical physics, a unique solution of a second-order partial differential equation is obtained only when the sought function or its first derivative is given along an entire contour bounding the region in question. The cutting off of the series in reference 32 therefore corresponds to fixing the carbon concentration at the pearlite surface in such a way that all coefficients except the first three will vanish. However, the carbon concentration at the pearlite-austenite interface must clearly have an equilibrium value determined by the curvature of the pearlite nucleus at the given point. These considerations make it desirable to devise a different scheme for calculating the growth rate of pearlite grains.[33]

The carbon concentration distribution ahead of the front of a pearlite transformation is described by a two-dimensional diffusion equation, which for a steady process in a coordinate system moving at velocity v with the front becomes

$$\frac{\partial^2 C}{\partial x^2} + \frac{\partial^2 C}{\partial y^2} + \frac{v}{D}\frac{\partial C}{\partial x} = 0. \tag{40}$$

The solution of this equation, taking into account the periodicity of concentration in the y direction, can be represented by

$$C(x, y) = C_0 + \sum_{n=1}^{\infty} K_n e^{-a_n x} \cos b_n y, \tag{41}$$

where $b_n = (2\pi/S_0)n$ and S_0 is the plate separation in pearlite. K_n and a_n are determined from (40) and the condition of mass balance at the interface, which is given approximately by

$$\frac{v}{D}[C_n(y) - C(0, y_0)] = \left(\frac{\partial C}{\partial x}\right)_{x=0}, \tag{42}$$

where y_0 is the coordinate on the interface and $C_n(y)$ is the carbon concentration distribution function in pearlite. Equation (42) is valid if we assume that the normal at any point of the austenite-pearlite interface is parallel to Ox. This simplification is equivalent to the assumption that in the range of x from the pearlite-austenite interface to the zOy plane the variation of carbon concentration in austenite can be neglected. In this way the true carbon distribution along the surface of a pearlite nucleus is "projected" on the zOy plane (Fig. 10). In addition to (42) we require

$$\left.\begin{aligned} C(0, 0) &= C_Q^c, \\ C\left(0, \frac{S_0}{2}\right) &= C_Q^f. \end{aligned}\right\} \tag{43}$$

It must also be remembered that $C_n(y)$ has the form shown in Fig. 12.

After a number of transformations we obtain, for the determination of

$$\alpha = \frac{4\pi D}{S_0 v}, \tag{44}$$

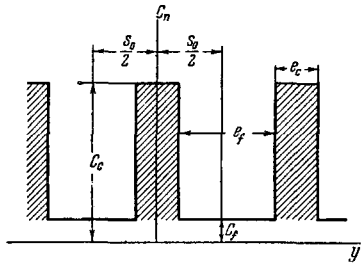

FIG. 12. Schematic diagram of the carbon distribution in pearlite.

the transcendental equation

$$\frac{C_Q^f - C_Q^c}{C_c - C_f} = \Phi(\alpha) = \frac{8}{\pi}\sum_{n=0}^{\infty}\frac{\sin\left[(2n+1)\pi\frac{C_0 - C_f}{C_c - C_f}\right]}{(2n+1)\left[\sqrt{1+(2n+1)^2\alpha^2}-1\right]}. \quad (45)$$

For $C_0 = 0.8\%$, $C_f = 0.04\%$, and $C_c = 6.67\%$, $\Phi(\alpha)$ is shown in Fig. 13.

Assuming the value of the carbon diffusion coefficient in austenite that was given in Eq. (26) and averaging in the indicated manner, we obtain $\overline{D(C)}$. We must also take[34]

$$S_0 = \frac{15}{996 - T}\cdot 10^{-4}\ \text{cm}. \quad (46)$$

Equation (44) is easily transformed into

$$v = \frac{4\pi D}{S_0\alpha}. \quad (47)$$

C_ρ^f and C_ρ^c are related to the radii of curvature of cementite-austenite and ferrite-austenite interfaces by Eqs. (38) and (39). The realized radii of curvature permit the system to approach equilibrium at a maximum rate, i.e., edgewise growth of pearlite grains proceeds at the maximum rate. Therefore, in accordance with (45), C_ρ^f must be as large as possible and C_ρ^c must be as small as possible. It follows from (38) and (39) that this condition requires a maximum radius of curvature at the center of the cementite-austenite interface ($\rho_c = \infty$) and a minimum radius of curvature at the center of the ferrite-austenite interface. The latter radius is that of the smallest ferrite grain according to our scheme, and is taken to be the critical nuclear radius ρ_{cr} for a γ-Fe $\rightarrow \alpha$-Fe transformation in pure iron. Therefore

$$C_Q^c = C_\infty^c, \qquad C_Q^f = C_\infty^f e^{v_c\frac{\sigma_{af}}{RTQ_{cr}}} = C_\infty^f e^{\frac{v_c}{v_{Fe}}\frac{\Delta F_0}{2RT}},$$

where we have taken $\sigma_{af} \approx \sigma_{fc}$, v_{Fe} is the atomic

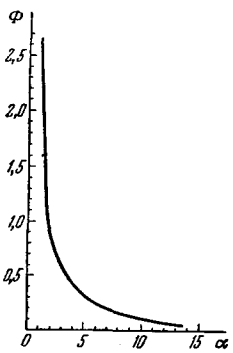

FIG. 13. The function $\Phi(\alpha)$.

FIG. 14. Edgewise growth rate of a pearlite grain vs. temperature. Solid curve – experimental; dashed curve – calculated.

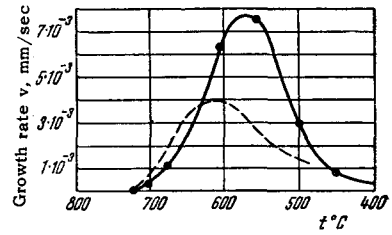

volume of iron, $\rho_{cr} = 2\sigma_{fc}/\Delta F_0$, and ΔF_0 is the change in free energy per gram-atom in the γ-Fe $\rightarrow \alpha$-Fe transformation. According to reference 15, in the temperature range of present interest experimental values for ΔF_0 can be expressed by

$$\Delta F_0 = RT\,[0{,}538 - (T - 273)\cdot 0{.}0007]. \quad (48)$$

Figure 14 shows fairly satisfactory agreement between calculations based on Eq. (47) (the dashed curve) and experimental results for industrial eutectoid steel.[35] However, the experimental result for the growth rate of a pearlite nucleus in the decomposition of high-purity eutectoid steel[36] is 10 – 15 times larger than the calculated value. Since our theoretical treatment neglected the effect of impurities, we now see that the decomposition of a solid solution is affected by an additional, accelerating factor that we failed to consider. This is confirmed by Fig. 5, where the experimental curve also lies above the theoretical curve. The omitted factor is obviously associated with the characteristics of solid-state phase transformations that are due mainly to anisotropy of the transformed substance and transformation-induced stresses.

3. The Influence of Transformation-Induced Stresses on the Growth Rate of Nuclei

In this section we discuss the influence of the aforementioned stresses on the growth rate of new-phase nuclei during the isothermal decomposition of solid solutions. Anisotropy of the medium will not be taken into consideration. The influence of the stresses on the kinetics of the process is complicated by the simultaneous effects of two factors. The presence of different atomic volumes of the new and old phases around a nucleus produces a stress field that is independent of the solute concentration. Also, an inhomogeneous concentration distribution around a nucleus resembles an inhomogeneous temperature distribution causing thermal stresses, and thus generates "concentration stresses." Both kinds of stresses have been studied by V. S. Gorskii,[37] S. T. Konobeevskii,[38,39] and M. I. Zakharov and N. F. Lashko.[40]

A differential equation for diffusion in a stress field is given in reference 38, and an analogous equation based on thermodynamic analysis was derived in reference 41:*

*The derivation of (49) is based on special considerations that are extraneous to the present discussion.

$$\frac{\partial C}{\partial t} = D\left(\Delta C - \frac{\omega C v_0}{RT}\Delta\sigma_{ll}\right). \quad (49)$$

It is assumed here that solute atoms change the lattice parameter of the solid solution according to the law

$$a = a_0[1 + \omega(C - C_0)]. \quad (50)$$

In this equation ω for substitutional solid solutions represents the difference between the atomic radii r_B and r_A of the solute and solvent, respectively, as follows:

$$\omega = \frac{r_B - r_A}{r_A}.$$

In interstitial solid solutions ω simply represents the dependence of the solvent lattice parameter on the solute concentration. The deformation of the solvent lattice around a nucleus, resulting from the presence of solute atoms with concentration C, is

$$\varepsilon_c^{\text{outer}} = \omega(C - C_0). \quad (51)$$

Within a nucleus we have, analogously,*

$$\varepsilon_c^{\text{inner}} = \omega(C_{\text{np}} - C_0). \quad (52)$$

Equations (51) and (52) can be used to calculate the stress tensor components in the case of a spherical nucleus, using the conventional methods applied to temperature stresses in the theory of elasticity.[42] Temperature is replaced formally by the concentration and the coefficient of thermal expansion by the quantity ω. Following some simple transformations we obtain for $r > \rho(t)$:

$$\sigma_r = -\frac{E\omega}{u^3}\left[C_{\text{np}} - C_0 + \int_1^u (C - C_0)\, d(\eta^3)\right],$$

$$\sigma_\tau = \frac{E\omega}{2u^3}\left[C_{\text{np}} - C_0 + \int_1^u (C - C_0)\, d(\eta^3) + 3(C_0 - C)u^3\right]. \quad (53)$$

Here $u = \frac{r}{\rho(t)}$ and E is the elastic modulus. Using (53), we obtain

$$\sigma_{ll} = \sigma_r + 2\sigma_\tau = -3E\omega(C - C_0). \quad (54)$$

The substitution of (54) in (49) gives us an equation for the diffusion of the solute around a nucleus, taking concentration stresses into account:

$$\frac{\partial C}{\partial t} = D'\left(\frac{\partial^2 C}{\partial r^2} + \frac{2}{r}\frac{\partial C}{\partial r}\right), \quad (55)$$

where $D' = D\left(1 + \frac{3\overline{C}v_0 E\omega^2}{RT}\right)$. The solution of this last equation is simplified by linearization, which is permissible since C varies over only a relatively small range. We therefore replace the true concentration with its average value

$$\overline{C} = \frac{C_\infty + C_0}{2}. \quad (56)$$

*We are neglecting here the deformation resulting from different types of atomic packing in the two phases.[39] This usually does not affect the calculated result.

It can easily be seen that (55) is mathematically identical with (14). For example, in the case of ferrite grain growth the solution of the former is given by (21) with D replaced by D'.

We introduce

$$\chi = \frac{\overline{C}v_0 E\omega^2}{RT}. \quad (57)$$

Then

$$D' = D(1 + 3\chi), \quad (58)$$

and the growth rate of a nucleus, taking concentration stresses into account, is

$$v = \frac{\beta\sqrt{\overline{D(C)}(1+3\chi)}}{\sqrt{t}}. \quad (59)$$

The difference between the specific volumes of the two phases produces stresses that shift the lines in the constitution diagram of the system; this will affect the value of β obtained from the transcendental equation (23). However, we shall neglect this effect since a calculation given in reference 43 shows that it is insignificant.

For the growth of the ferrite grain considered above at 720° C and $C_0 = 0.022$ atomic fraction (or 0.5 weight %) we have $\sqrt{1 + 3\chi} = 1.27$. The ratio of ferrite grain growth calculated from (59) is compared in Fig. 15 with the growth rate as calculated neglecting stresses, and also with experimental findings, which are more nearly approximated when stresses are taken into account.

We shall now calculate the stress field around spherical nuclei. Substituting in (53) the expression (21) for the concentration field with D replaced by D', we obtain by integrating,

$$\sigma_r = -\frac{E\omega}{u^3}(C_\infty - C_0)\left[\frac{u^3 f(u\beta)}{f(\beta)} + \frac{e^{-\beta^2} - e^{-u^2\beta^2}}{2\beta^3 f(\beta)} - 1 + \frac{C_{\text{np}} - C_0}{C_\infty - C_0}\right],$$

$$\sigma_\tau = -\frac{E\omega}{u^3}(C_\infty - C_0)\left[\frac{u^3 f(u\beta)}{f(\beta)} - \frac{1}{2}\left(\frac{e^{-\beta^2} - e^{-u^2\beta^2}}{2\beta^3 f(\beta)} - 1 + \frac{C_{\text{np}} - C_0}{C_\infty - C_0}\right)\right], \quad (60)$$

where

$$f(x) = \frac{e^{-x^2}}{x} - 2\int_x^\infty e^{-\xi^2}\, d\xi.$$

Figure 16 shows the results obtained from (60) for ferrite grain growth with the parameters $C_0 = 0.5\%$, $\beta = 0.8$, $T = 993°$, $E = 2 \times 10^4$ kg/mm^2, and $\omega = 0.2$. Radial tensile stresses ($\sigma_r > 0$) appear on the sur-

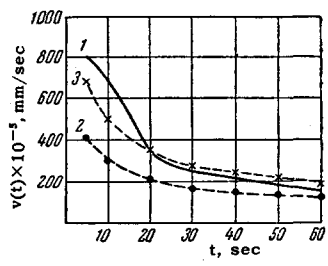

FIG. 15. Growth rate of a ferrite grain at 720°C. Curve 1 – experimental; curve 2 – calculated neglecting stresses; curve 3 – calculated including stresses.

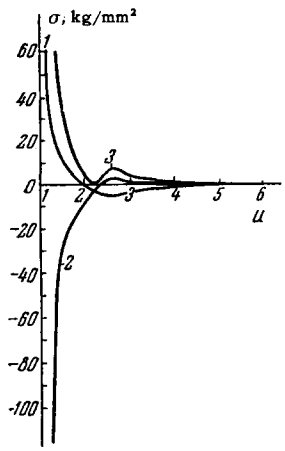

FIG. 16. Stress distribution near a growing ferrite grain. 1 – radial component σ_r; 2 – tangential component σ_τ; 3 – values of $|\sigma_r - \sigma_\tau|$.

face of a nucleus up to u ≅ 2, after which σ_r becomes negative. Tangential stresses σ_τ near the surface of a nucleus are negative and are reversed at u = 2.3. It is especially interesting to study the absolute value of the difference $|\sigma_r - \sigma_\tau|$, since the condition for a plastic transition of the substance can be given as[44]

$$|\sigma_r - \sigma_\tau| \geqslant \sigma_s, \tag{61}$$

where σ_S is the yield point determined from tests on macroscopic samples. In our case

$$|\sigma_r - \sigma_\tau| = \frac{3}{2}\frac{E\omega}{u^3}(C_\infty - C_0)\left[\frac{e^{-\beta^2} - e^{-u^2\beta^2}}{2\beta^3 f(\beta)} - 1 + \frac{C_{np} - C_0}{C_\infty - C_0}\right]. \tag{62}$$

Figure 16 shows that $|\sigma_r - \sigma_\tau|$ is very large near the nuclear surface, but decreases rapidly, vanishing at u = 2.2, after which there is some increase.

If σ_S is taken as 10 kg/mm², in accordance with mechanical tests at high temperatures, a plastic state is produced only in the immediate vicinity of nuclear surfaces. It should be noted that the given value of σ_S is assumed arbitrarily, since it is at present not entirely clear to what extent mechanical properties derived from experiments on macroscopic samples can be applied to the range of very small dimensions. X-ray determinations of the elastic modulus suggest that this modulus is approximately identical for volumes of different orders of smallness. No analogous statement is justified regarding σ_S, for which a detailed study of the mechanism of plastic deformation in microscopic volumes is required. The modern dislocation theory[45] suggests that the yield point in microscopic volumes is considerably above the value assumed by us. Plastic deformation at the surface of a nucleus leads to partial relaxation of the concentration stresses and therefore diminishes their effect on the nuclear growth rate.

It follows from the foregoing that when a nucleus is growing in undercooled austenite the stresses induced by the phase transformation itself exercise an autocatalytic influence on the growth process. An especially marked effect of concentration stresses can be expected in the decomposition of eutectoid solid solutions. Large changes of concentration within small volumes induce appreciable stresses within the decomposition product, and also in the initial solid solution as a result of interactions between the phases.

We shall illustrate our hypothesis by calculating the edgewise growth of pearlite grains taking account of concentration stresses.[46,47] The diffusion of the solute in the stress field is described by (49), which we represent approximately[39] by

$$\frac{\partial C}{\partial t} = \operatorname{div}(D' \operatorname{grad} C) - \operatorname{div}(D'' \operatorname{grad}\varepsilon);$$

$$\varepsilon = \frac{\varepsilon_{xx} + \varepsilon_{yy} + \varepsilon_{zz}}{3},$$

$$D' = D\left(1 + \frac{3v_0 L\omega^2}{\frac{\partial^2 F_0}{\partial C^2}}\right), \quad D'' = D\frac{3v_0 L\omega}{\frac{\partial^2 F_0}{\partial C^2}}, \tag{63}$$

where F_0 is the free energy of the solid solution in the absence of stresses, expressed in cal/gram-atom; $L = E/(1-2\nu) = 3E$, since the Poisson coefficient is $\nu = 1/3$; ϵ_{xx}, ϵ_{yy}, and ϵ_{zz} are the strain tensor components.

In the approximation of dilute solutions we obtain

$$\frac{\partial^2 F_0}{\partial C^2} = \frac{RT}{C}, \quad D' = D\left(1 + \frac{9v_0 E\omega^2 C}{RT}\right),$$
$$D'' = D\frac{9v_0 E\omega C}{RT}. \tag{64}$$

We shall now calculate the edgewise growth rate of a pearlite nucleus if diffusion processes in austenite are represented by (63). We transform to coordinates moving with velocity v along the x axis and consider the carbon concentration to be constant ahead of the phase transformation front during the process (Fig. 10). Equation (63) then becomes

$$\operatorname{div}(D' \operatorname{grad} C) - \operatorname{div}(D'' \operatorname{grad}\varepsilon) + v \operatorname{grad} C = 0. \tag{65}$$

We must know how ϵ depends on C in order to solve (65). As already mentioned, this problem in the theory of elasticity can be solved by methods used for thermoelastic stresses.[42] It is necessary to obtain the auxiliary function $U_1 - T_1$, where

$$\nabla^4 U_1 = 0, \quad \nabla^2 T_1 = E\omega(C - C_0). \tag{66}$$

The concentration distribution in austenite is here given by a formula analogous to (41). We shall now determine the coefficients K_n and a_n, which are considerably complicated in the present case.

We begin by seeking the function T_1, which can obviously be represented by

$$T_1 = \sum_{n=0}^{\infty} \psi_n(x) \cos b_n y, \tag{67}$$

where $b_n = (2\pi/s_0)n$. Substituting (67) in the second equation of (66), we obtain the solution*

$$\psi_n(x) = A_n e^{b_n x} + B_n e^{-b_n x} + \frac{E\omega}{b_n}\int_x^{\infty} K_n e^{-a_n \xi} \operatorname{sh} b_n(x - \xi)\, d\xi. \tag{68}$$

Since for $x \to \infty$ all components of the stress tensor must approach zero, we have $A_n = 0$. U_1 is written in the form

*sh = sinh.

$$U_1 = \sum_{n=0}^{\infty} W_n(x)\cos b_n y. \tag{69}$$

The function $W_n(x)$ is obtained by solving the equation resulting from the substitution of (69) in the first equation of (66). In virtue of the aforementioned condition when $x \to \infty$, we have

$$W_n(x) = (M_n + N_n x)\, e^{-b_n x}, \tag{70}$$

where M_n and N_n are arbitrary constants.

With U_1 and T_1 known, we obtain the following stress tensor components in a supersaturated solid solution:

$$\left.\begin{aligned}
\sigma_{xx} &= \frac{\partial^2 (U_1 - T_1)}{\partial y^2} = \sum_{n=0}^{\infty} \Big[-b_n^2 (N_n x + L_n)\, e^{-b_n x} \\
&\quad + E\omega b_n \int_0^x K_n e^{-a_n \xi} \operatorname{sh} b_n (x-\xi)\, d\xi \Big] \cos b_n y, \\
\sigma_{yy} &= \frac{\partial^2 (U_1 - T_1)}{\partial x^2} = \sum_{n=0}^{\infty} \Big[b_n^2 (N_n x + L_n)\, e^{-b_n x} - 2N_n b_n e^{-b_n x} \\
&\quad - E\omega\varphi_n(x) - E\omega b_n \int_0^x K_n e^{-a_n \xi} \operatorname{sh} b_n (x-\xi)\, d\xi \Big] \cos b_i y, \\
\tau_{xy} &= -\frac{\partial^2 (U_1 - T_1)}{\partial x\, \partial y} = \sum_{n=0}^{\infty} \Big[b_n^2 (N_n x + L_n)\, e^{-b_n x} - b_n N_n e^{-b_n x} \\
&\quad + E\omega b_n \int_0^x K_n e^{-a_n \xi} \operatorname{sh} b_n (x-\xi)\, d\xi \Big] \sin b_n y.
\end{aligned}\right\} \tag{71}$$

The components of the strain tensor are related to σ_{xx} and σ_{yy} by

$$\left.\begin{aligned}
\varepsilon_{xx} &= \frac{1-\nu^2}{E}\sigma_{xx} - \frac{\nu(1+\nu)}{E}\sigma_{yy} + (1+\nu)\,\omega (C - C_0), \\
\varepsilon_{yy} &= \frac{1-\nu^2}{E}\sigma_{yy} - \frac{\nu(1+\nu)}{E}\sigma_{xx} + (1+\nu)\,\omega (C - C_0), \\
\varepsilon_{zz} &= 0.
\end{aligned}\right\} \tag{72}$$

In the expressions in Eq. (64) for D' and D'' we replace C with $\overline{C}$, where

$$\overline{C} = \frac{C_0 + C_0^c + C_0^f}{3}.$$

Equation (65) then becomes

$$D'\Delta C - D''\Delta\varepsilon + v\,\operatorname{grad} C = 0. \tag{73}$$

On the basis of (72) and expressing the concentration by (41), we obtain the following equation for a_n:

$$\left(D' - \frac{20}{27}D''\omega\right)a_n^2 - va_n - \left(D' - \frac{20}{27}D''\omega\right)b_n^2 = 0, \tag{74}$$

whence

$$a_n = \frac{v}{2D_{\text{eff}}}\left(1 + \sqrt{1 + \lambda^2 n^2}\right), \tag{75}$$

$$D_{\text{eff}} = D' - \frac{20}{27}D''\omega = D\left(1 + \frac{7}{27}\beta\right), \tag{76}$$

$$\beta = \frac{9v_0 E\omega^2 \overline{C}}{RT}, \qquad \lambda = \frac{4\pi D_{\text{eff}}}{S_0 v}. \tag{77}$$

When concentration stresses are taken into account, Eq. (42) becomes

$$[C_n(y_0) - C(0, y_0)]\, v = D'\left(\frac{\partial C}{\partial x}\right)_{x=0} - D''\left(\frac{\partial \varepsilon}{\partial x}\right)_{x=0}. \tag{78}$$

Substituting (72) and (41) for C in (78), we obtain the following equation for K_n with $n \geq 1$:

$$v(\gamma_n - K_n) + K_n a_n D' + \frac{8}{27}\frac{b_n^2}{E}D''N_n - \frac{20}{27}a_n K_n D''\omega = 0. \tag{79}$$

The carbon distribution in pearlite is here represented by

$$C_n(y) = C_0 + \sum_{n=1}^{\infty} \gamma_n \cos b_n y$$
$$\left(\gamma_n = \frac{2(C_c - C_f)}{\pi n} \sin\left(n\pi \frac{l_c}{S_0}\right)\right) \tag{80}$$

Equation (80) corresponds to the scheme shown in Fig. 12. Equation (79) contains the unknown coefficients N_n, which we shall determine from the equality of the normal stresses σ_{xx} and displacements u at an interface.

It follows from (71) that on the austenite side of an interface we have

$$(\sigma_{xx})_{x=0} = \sum_{n=0}^{\infty}\left(-b_n^2 L_n + \frac{E\omega K_n}{a_n^2 - b_n^2}\, b_n^2\right)\cos b_n y, \tag{81}$$

since

$$\int_0^x e^{-a_n \xi} \operatorname{sh} b_n (x-\xi)\, d\xi = \frac{b_n}{a_n^2 - b_n^2}\, e^{-a_n x}.$$

The complex character of pearlite, resulting from the fact that it consists of lamellae having two different structures, makes it impossible to calculate concentration stresses using the theory of thermoelasticity. However, as a first approximation it will also be assumed in this case that we are seeking functions U_1 and T_1 satisfying the equations

$$\frac{d^4 U_1}{dy^4} = 0, \qquad \frac{d^2 T_1}{dy^2} = E\omega\,[C_n(y) - C_0]. \tag{82}$$

From the solution of (82) and equilibrium conditions at the phase front

$$\int_0^{S_0} \sigma_{xx}\, dy = 0, \tag{83}$$

we obtain

$$\sigma_{xx} = -E\omega \sum_{n=1}^{\infty} \gamma_n \cos b_n y. \tag{84}$$

From (84) and (81) we obtain

$$L_n = E\omega\left(\frac{K_n}{a_n^2 - b_n^2} + \frac{\gamma_n}{b_n^2}\right). \tag{85}$$

The displacement in pearlite is

$$u_n = \int_0^x \varepsilon_{xx}\, dx, \tag{86}$$

where

$$\varepsilon_{xx} = \frac{1}{E}\sigma_{xx} + \omega\,[C_n(y) - C_0].$$

Hence

$$u_n = 0. \tag{87}$$

u_a in austenite is determined from the relationship between displacements and stresses:

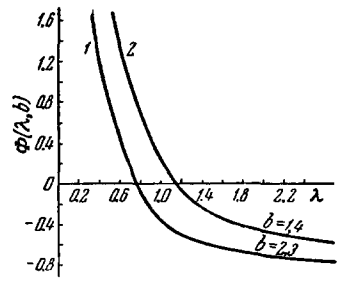

FIG. 17. $\Phi(\lambda, b)$ for b = 2.3 (curve 1) and b = 1.4 (curve 2).

$$u_a = \frac{1-\nu^2}{E}\int_0^x \sigma_{xx}\,dx - \frac{\nu(1+\nu)}{E}\int_0^x \sigma_{yy}\,dx + (1+\nu)\,\omega\int_0^x (C-C_0)\,dx. \tag{88}$$

In virtue of (71), (85), and (87) we obtain

$$N_n = E\omega\left[K_n\frac{4a_n+b_n}{a_n(a_n+b_n)} - 3\frac{\gamma_n}{b_n}\right]. \tag{89}$$

The substitution of (79) in (89) leads to the solution

$$K_n = \gamma_n \frac{1-\frac{12}{27}\,b\lambda n}{\frac{1}{2}-\frac{1}{2}\,C^n(\lambda)-\frac{4}{27}\,b\,\frac{\lambda^2n^2[4+4C^n(\lambda)+\lambda n]}{[1+C^n(\lambda)][1+C^n(\lambda)+\lambda n]}},$$

$$C^n(\lambda) = \sqrt{1+\lambda^2n^2}, \quad b = \frac{D''\omega}{D_{\text{eff}}}. \tag{90}$$

We have thus obtained a function C(x, y) for the carbon concentration distribution in austenite. From the conditions (43) we have

$$C_0 + K_0 + \sum_{n=1}^{\infty} K_n = C_0^c, \tag{91}$$

$$C_0 + K_0 + \sum_{n=1}^{\infty} (-1)^n K_n = C_0^f. \tag{92}$$

Subtracting (91) from (92) and substituting for γ_n, we have

$$\Phi(\lambda, b) = \frac{8}{\pi}\sum_{n=0}^{\infty} \frac{\left[1-\frac{12}{27}\,b\lambda m\right]\frac{\sin\frac{\pi l_c}{S_0}m}{m}}{C^m(\lambda)-1+\frac{8}{27}\,b\,\frac{\lambda^2m^2[4+4C^m(\lambda)+\lambda m]}{[1+C^m(\lambda)][1+C^m(\lambda)+\lambda m]}}$$

$$= \frac{C_0^f - C_0^c}{C_c - C_f}, \quad m = 2n+1. \tag{93}$$

The value of b depends on the transformation temperature, varying from 1.4 to 2.3 in the temperature range from 723 to 500° C. Figure 17 shows $\Phi(\lambda, b)$ for b = 2.3 (curve 1) and b = 1.4 (curve 2). Curve 1 in Fig. 18 shows the edgewise growth rate of a pearlite grain calculated from

$$v = \frac{4\pi D_{\text{eff}}}{S_0\lambda} \tag{94}$$

as a function of temperature. Curve 3 is obtained from Eq. (47) (b = 0). The figure also shows experimental findings for two industrial eutectoid steels (curves 4 and 5)[35] and for a high-purity eutectoid steel with 0.93% C, 0.002% Si, and < 0.004% Mn (curve 2).[36] The theoretical value of the edgewise growth rate is considerably enhanced by taking concentration stresses into account, and approaches the experimental value.

When the carbon concentration distribution is known it is not difficult to determine the corresponding concentration stresses,[48] which are represented analytically by

$$\begin{aligned}
\sigma_{xx} &= E\omega\sum_{n=1}^{\infty}\left\{\left[\left(3b_n\gamma_n - \frac{K_nb_n^2(4a_n+b_n)\,x}{a_n(a_n+b_n)}\right)\right.\right.\\
&\quad\left.-\gamma_n - \frac{K_nb_n^2}{a_n^2-b_n^2}\right]e^{-b_nx} + \frac{K_nb_n^2e^{-a_nx}}{a_n^2-b_n^2}\Big\}\cos b_ny,\\
\sigma_{yy} &= -E\omega K_0e^{-a_0x} + E\omega\sum_{n=1}^{\infty}\left\{\left[\left(\frac{K_nb_n^2(4a_n+b_n)}{a_n(a_n+b_n)} - 3\gamma_nb_n\right)x\right.\right.\\
&\quad+\frac{K_nb_n^2}{a_n^2-b_n^2} + 4\gamma_n - \frac{2K_nb_n(4a_n+b_n)}{a_n(a_n+b_n)}\Big]e^{-b_nx}\\
&\quad\left.-\frac{K_na_n^2e^{-a_nx}}{a_n^2-b_n^2}\right\}\cos b_ny,\\
\tau_{xy} &= E\omega\sum_{n=1}^{\infty}\left\{\left[\left(3b_n\gamma_n - \frac{K_nb_n^2(4a_n+b_n)}{a_n(a_n+b_n)}\right)x - \frac{K_nb_n^2}{a_n^2-b_n^2} - 4\gamma_n\right.\right.\\
&\quad\left.+\frac{K_nb_n(4a_n+b_n)}{a_n(a_n+b_n)}\Big]e^{-b_nx} + \frac{K_na_nb_n}{a_n^2-b_n^2}e^{-a_nx}\right\}\sin b_ny.
\end{aligned} \tag{95}$$

These equations are used to plot curves representing the concentration stress distribution ahead of the pearlite transformation front (Fig. 19 a-c). The condition for the plastic transition is now given by reference 44

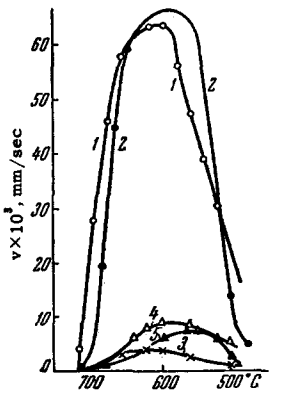

FIG. 18. Edgewise growth rate of a pearlite grain. 1 – theoretical from (94); 3 – theoretical from (47); 2 – experimental for high-purity eutectoid steel; 4, 5 – experimental for industrial steels.

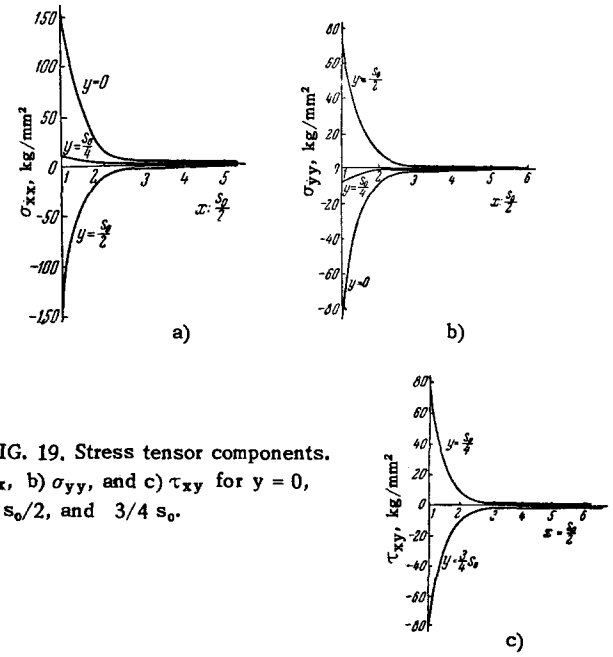

FIG. 19. Stress tensor components. a) σ_{xx}, b) σ_{yy}, and c) τ_{xy} for y = 0, $s_0/4$, $s_0/2$, and 3/4 s_0.

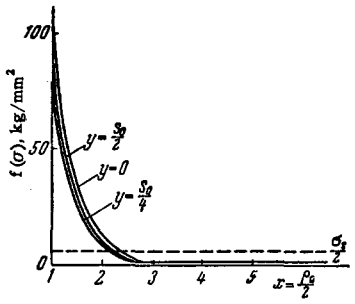

FIG. 20. Condition for plastic deformation at a pearlite front. Dashed line – for $\sigma_s/2$.

$$f(\sigma)=\sqrt{\frac{1}{4}(\sigma_{xx}-\sigma_{yy})^2+\tau_{xy}^2}\geqslant\frac{\sigma_s}{2}. \qquad (96)$$

Figure 20 shows the extent of the region outside of an interface in which plastic deformation can occur. As in the case of a spherical nucleus, plastic flow partially relaxes the concentration stresses and thus reduces their influence.

4. The Decomposition Kinetics of Supersaturated Binary Solid Solutions

There are two factors determining the kinetics of phase transformations in binary solid solutions. These are the reconstruction rate of the solvent lattice and the solute diffusion rate. As a specific problem we shall consider the precipitation of ferrite from undercooled hypoeutectoid austenite. As already shown, up to $\rho=\rho_{lim}>\rho_{cr}$ the rate of the process is determined by the reconstruction of the iron lattice, while for $\rho>\rho_{lim}$ the limiting factor is carbon diffusion. If τ is the time required for a nucleus to grow to the radius ρ_{lim}, the growth rate of a ferrite nucleus is given by (4), and for $t>\tau$ by (17). Nucleation takes place as in a one-component system and is represented by Eq. (3). For the general case we thus obtain[49]

$$t_\eta=\left[-\frac{15h\ln(1-\eta)}{8\pi RTD_0^{3/2}\beta^3}\exp\left(\frac{W+U+\frac{3}{2}Q}{RT}\right)-\frac{5\pi^3d^{12}(\Delta F_0)^3\tau^4}{8\cdot3^6h^3D_0^{3/2}\beta^3}\exp\left(\frac{\frac{3}{2}Q-3U}{RT}\right)+\tau^{5/2}\right]^{2/5} \qquad (97)$$

For $t\ll\tau$ the reconstruction rate determines the transformation kinetics, which is represented by (10). When the carbon diffusion rate is the limiting factor we have

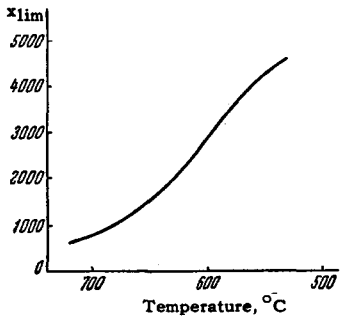

FIG. 21. x_{lim} in carbon steel at different temperatures.

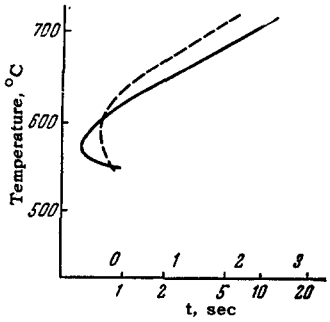

FIG. 22. Curves for the kinetics of isothermal austenite decomposition in unalloyed steel. Solid curve – experimental; dashed curve – calculated. (This was a 5% transformation.)

$$t_\eta=\left[-\frac{15h\ln(1-\eta)}{8\pi RT\beta^3D_0^{3/2}}\right]^{2/5}\cdot\exp\left[\frac{\frac{2}{5}(W+U)+\frac{3}{5}Q}{RT}\right]. \qquad (98)$$

Equation (18) is used to calculate $x_{lim}=\rho_{lim}/\rho_{cr}$. We assume $C_0=0.5\%$ and obtain $D_0=0.1$ cm²/sec from (26). The activation energy for the γ-Fe $\rightarrow$ α-Fe transformation in carbon steel is taken to be the average of the activation energies for recrystallization in α- and γ-iron.[50] The results are U = 35 kcal/mole, with $r_a=1.25\times10^{-8}$ cm. The value of σ has practically no effect on the determination of ρ_{lim}, which is usually considerably larger than ρ_{cr}; σ affects only the latter. An indirect calculation shows that in our case x_{lim} increases at lower temperatures as shown in Fig. 21. Thus, while carbon diffusion is the limiting process down to 650° C, the importance of the lattice reconstruction mechanism increases in the range 650 – 600° C and becomes the controlling factor below 600° C. It follows that the kinetics of the transformation can be calculated from (98) down to 650° C, but that (97) must be used at lower temperatures.

The solid curve in Fig. 22 represents the kinetics of the 5% austenite transformation of steel containing 0.45% carbon,[51] while the dashed curve represents the corresponding calculation. The calculation required knowledge of the value of σ in W. σ is not known exactly and will be considered a free theoretical parameter. An indirect confirmation of the correctness of our reasoning is provided by the reasonable order of magnitude of σ, giving satisfactory agreement between the calculations and experiment. In our case*

$$\sigma=40+0.36(996-T). \qquad (99)$$

Although ΔF_0 depends on the carbon content, in the present calculation we assume as an approximation that Eq. (48) represents the change of free energy in the $\gamma\rightarrow\alpha$ transformation.

The kinetics of the pearlite transformation can be analyzed by comparing the theoretical kinetic curves with experimental results.[52] A calculation of the kinetics of the pearlite transformation with the rate of lattice reconstruction as the controlling factor is represented by curve 2 in Fig. 23. In the calculation 0.8% carbon content was taken for the eutectoid steel. Since

*In all subsequent formulas σ is given in erg/cm².

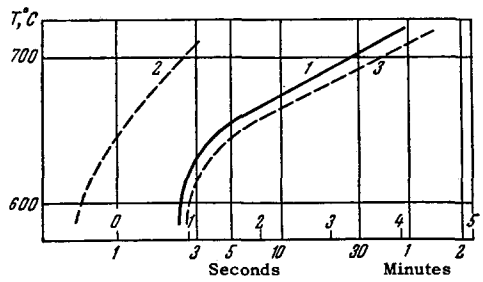

FIG. 23. Kinetics of the isothermal (pearlite) decomposition of austenite in unalloyed steel. (This was a 50% transformation.) 1 – experimental; 2 – calculated with the $\gamma \rightarrow \alpha$ lattice transformation as the controlling process; 3 – calculated with carbon diffusion as the controlling process.

a higher carbon content reduces the activation energy for iron self-diffusion according to the law[53]

$$U = U_0(1 - 0.4C\%), \qquad (100)$$

in our case we have U = 30 kcal/mole (U_0 = 45 kcal/mole).

In the kinetic calculation we assume that pearlite nuclei grow as spheres. This assumption is based on the approximate equality of the edgewise and sidewise growth rates of pearlite.[54] Curve 3 of Fig. 23 shows the result of a calculation with carbon diffusion as the limiting process, taking account of concentration stresses. Curve 1 is based on an experimental investigation of the pearlite transformation in plain carbon steel (η = 0.5). In this case the pearlite transformation is clearly not limited by the rate of the $\gamma \rightarrow \alpha$ polymorphic transformation and is therefore controlled by carbon diffusion. Since cementite was taken to be the leading phase the calculation required a value of the surface tension at the austenite-cementite interface; it was assumed that

$$\sigma_{ac} = 48 + 0.3(993 - T). \qquad (101)$$

It should be noted that the somewhat arbitrary values of σ used in the present work and any possibly refined values for free-energy changes accompanying nucleation cannot affect our general conclusions, since the pertinent equations contain the same power of the work of formation W of a critical nucleus, and therefore do not determine the relative positions of the calculated curves 2 and 3.[52]

The results of the present investigation show that the hypothesis in reference 55 to the effect that the lattice reconstruction mechanism controls the eutectoid transformation in unalloyed carbon steel is not valid in the range 723 – 600° C. This hypothesis was advanced in reference 55 because the conventional explantion based on the carbon diffusion mechanism did not explain the pearlite transformation in high-purity unalloyed eutectoid steels. Allowance for the way in which diffusion is affected by the concentration stresses arising in the pearlite transformation leads to good

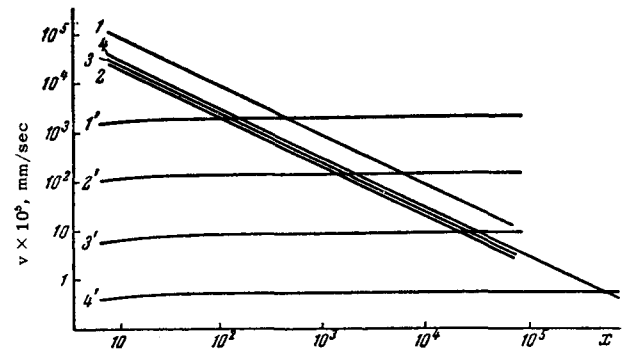

FIG. 24. Graphs corresponding to (4) and (24) for determining x_{lim} for ferrite grain growth in unalloyed steel (1) and in chromium steels (2, 3, 4) containing 3%, 6%, and 9% chromium, respectively, at 720°C.

agreement between experiment and the pearlite growth rate calculated from (94). On the other hand, in reference 55 empirical constants are chosen in order to establish an artificial connection between the experimental curves and Eq. (7) for pearlite growth.

IV. TERNARY SYSTEMS

In connection with the decomposition of a supersaturated ternary solid solution it is necessary first to determine the effect of the third element on x_{lim}. This effect appears in changes of C_∞, C_{np}, U, Q, D_0, and σ. As an illustration we shall consider the kinetics of the austenite decomposition of hypoeutectoid alloy steel, i.e., of a system containing iron, carbon, and an alloying element such as Cr or Mo. The alloying element changes the positions of phase boundaries in the alloy equilibrium diagram, and therefore changes C_∞ and C_{np}. The presence of the alloying element also changes the foregoing process parameters U, Q, D_0 and σ. Our thesis is subject to the condition that diffusion of the alloying element does not itself inhibit the process.

We shall calculate the change of x_{lim} at 720° C for different chromium contents (with 0.5% carbon content). Curves 1 – 4 in Fig. 24 show the dependence of $d\rho/dt$ on x calculated from (24); curves 1′ – 4′ were calculated from (4). The intersections of the corresponding curves (1-1′, 2-2′, 3-3′, 4-4′) determine x_{lim} for each steel. C_∞ and C_{np} are obtained from the constitution diagram,[56] by extrapolating to low temperatures the boundary of the γ region for a given content of the alloying component. For example, with 5% Cr we have

$$C'_\infty = 0.48 + 0.016(1083 - T). \qquad (102)$$

The effect of alloying on D_0 and Q is considered in reference 57. In alloys containing up to 7% chromium, D_0 increases to 0.21 cm²/sec, and Q increases to 38 900 cal/mole. A study of the available data[58] indicates that the ferrite-austenite surface tension decreases in an alloy (to 20 erg/cm² in the case of chromium). We take

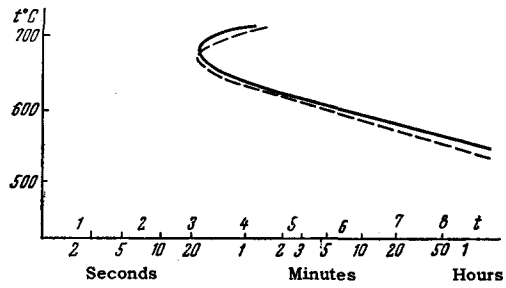

FIG. 25. Kinetics of isothermal austenite decomposition in steel containing 0.4% C and 8.5% Cr (a 5% transformation). Solid curve – experimental; dashed curve – calculated.

$$\sigma_{af} = 22 + 0.3(993 - T). \tag{103}$$

Our calculation of ΔF_0 follows:[31]

$$\Delta F_0 = N_{Fe}\,\Delta F_{Fe}^{\gamma\to\alpha} + N_C\,(10500 - 3.425T) + \Delta F_* + \sum N_i K_i, \tag{104}$$

where N_i is the mole fraction of an alloying element, K_i are temperature-dependent alloying constants, and the other quantities are the same as in (37). For a chromium alloy[49] we have

$$K_i(T) = 1200 - 1.5(T - 500). \tag{105}$$

The change of U in alloys is arbitrarily taken to represent the way in which the activation energy for iron self-diffusion in austenite[57] depends on alloying. For chromium alloys this dependence is represented analytically by

$$U = U_0(1 + 0.044C), \tag{106}$$

which agrees with experiment. Alloying considerably increases x_{lim}, which even at 720° with 6% Cr has a value of the order of tens of thousands. Thus in the kinetics of the austenite transformation in chromium steel the limiting process is the mechanism of lattice reconstruction, and the kinetic curve is represented by Eq. (10).

The solid curve in Fig. 25 represents a 5% austenite transformation in steel containing 0.4% C and 8.5% Cr according to data given in reference 59. The dashed curve represents a calculation based on Eq. (10). Some other alloying elements appear to have a similar effect on the kinetics of ferrite precipitation from austenite.

We shall now consider how changes of the carbon content affect the kinetics of ferrite precipitation from undercooled austenite. In this case it is convenient to base an analysis of the limiting mechanism on the time when a nucleus attains its limiting size:[60]

$$\tau = \frac{\varrho_{lim}^2}{4\beta^2 D} = D_0\left(\frac{C_\infty^t - C_{np}}{C_0 - C_{np}}\right)^2\left(\frac{27h}{32\pi r_a^4 \beta \Delta F_0}\right)^2 \exp\left(\frac{2U - Q}{RT}\right). \tag{107}$$

The calculation of τ shows that the condition $\tau \gg t$ already given for the applicability of (10) is fulfilled in this case.

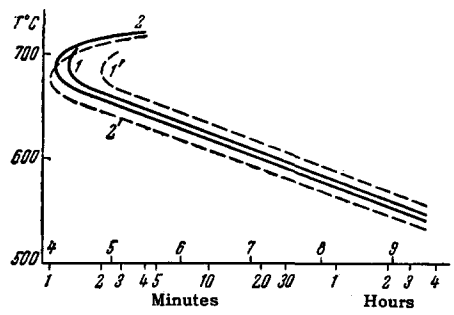

FIG. 26. Kinetics of isothermal austenite decomposition in steel alloys (a 5% transformation). Experimental: 1 – 8.5% Cr and 0.05% C; 2 – 8.5% Cr and 0.04% C. Calculated: 1′ – 8.5% Cr and 0.05% C; 2′ – 8.5% Cr and 0.04% C.

The dashed curves in Fig. 26 represent calculations based on (10): 1′ for steel containing 0.05% C and 8.5% Cr, and 2′ for steel containing 0.04% C and 8.5% Cr ($\eta = 0.05$). The solid curves 1 and 2 represent data given in reference 59 for the austenite transformation in these steels. Equation (106) gives U_0 = 58 kcal/mole for this steel. The values of σ_{af} at 720° are 17 and 22 ergs/cm^2, respectively. In alloy steels the effect of carbon on the activation energy for the γ-Fe $\rightarrow$ α-Fe lattice transformation is opposite that of alloying metals such as chromium. This also applies to the magnitude of the interface surface tension σ_{af}. The experimentally observed acceleration of the austenite transformation with increasing carbon content in steel alloys can be accounted for by the fact that an increase of the work of formation of a critical nucleus resulting from the increase of σ_{af} or the decrease of ΔF_0 does not cover the reduction of U, since the exponent in (10) contains $\frac{1}{4}$ W. Otherwise the austenite transformation in steel alloys would be slowed down.

With increasing carbon content there is only a small reduction of the activation energy for lattice reconstruction, but there is a considerable rise in the surface tension. In the transformation kinetics represented by (98) the controlling factor is the slowing-down of diffusion processes (through the value of β) and the austenite decomposition rate is decreased as a whole.

In order to determine the influence of alloying elements on the kinetics of the pearlite transformation it is necessary to learn the dependence of I and v on the concentration of alloying additions and on the transformation temperature T. According to current ideas regarding the pearlite transformation mechanism in steel alloys,[61] pearlite growth proceeds either without preliminary diffusion of the alloying element in austenite, or it is directly associated with the redistribution of that element. In the first case the eutectoid decomposition results in a two-phase lamellar structure of ferrite and cementite with spacing S_0, while the content of the alloying element differs little from that in

the original austenite. In the second case the new lamellar structure consists of ferrite and carbide, and the appearance of a pearlite colony will be regarded as beginning with the creation of carbide nuclei such as $(FeMe)_7C_3$ or $(FeMe)_3C$, as described by (3).

The edgewise growth rate of a pearlite grain in the original austenitic alloy is determined by the speed of the slowest process required for the eutectoid transformation. When a ferrite-cementite structure is formed, the processes involved are the reconstruction of the iron lattice and the diffusion of carbon. When a ferrite-carbide mixture is formed directly, another process is the diffusion of the alloying element, resulting in its high concentration in the carbide.

Equation (7) describes the growth rate of a pearlite nucleus when lattice reconstruction is the controlling process. Alloying increases considerably the activation energy for this process. By a calculation based on (7), the pearlite growth rate for a eutectoid transformation in unalloyed steel at 700° is 0.03 cm/sec, which is hundreds of times larger than the experimental value. In chromium steel (8.5% Cr, U_0 = 47 kcal/mole) the growth rate is calculated to be 10^{-5} cm/sec, which is considerably closer to the experimental result. Thus the introduction of an alloying element can slow the lattice transformation of the basic component, with the latter process limiting the transformation kinetics of the three-component solid solution.

The growth rate of pearlite grains as a result of carbon diffusion in an austenitic alloy will be calculated from (94). According to (76) and (77),

$$v = \frac{4\pi D_0}{S_0\lambda}\left(1+\frac{7}{3}\frac{v_0\bar{C}E\omega^2}{RT}\right)e^{-\frac{Q}{RT}}. \qquad (108)$$

In this equation alloying changes the quantities D_0, Q, S_0, λ, b, C_{ac}, C_{af}, and C_c (in the formation of carbides). For chromium steel (8.5% Cr) the pearlite growth rate calculated from (108) exceeds the experimental result.

In calculating the pearlite growth rate limited by the diffusion of the alloying element in austenite we proceeded as in the foregoing case with carbon diffusion as the limiting process, but with all parameters now pertaining to the migration of the alloying atoms. For the growth rate we obtain

$$v = \frac{4\pi D_{0k}}{\lambda_k S_0}(1+k)e^{-\frac{Q_k}{RT}}, \qquad (109)$$

where D_{0k} and Q_k are the diffusion parameters of the alloying element in austenite, λ_k is determined from

$$\Phi(\lambda_k,\ b) = \frac{C_Q^f - C_Q^k}{C_k - C_f}, \qquad (110)$$

which is similar to (93), and k is a correction taking concentration stresses into account. As was shown in reference 52,

$$v < \frac{80\pi D_{0k}}{S_0}e^{-\frac{Q_k}{RT}} \qquad (111)$$

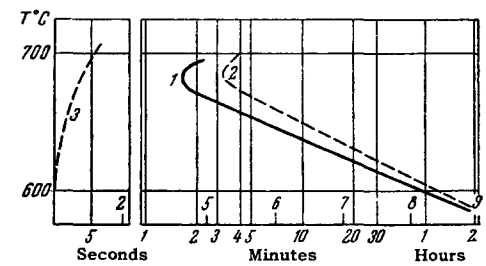

FIG. 27. Kinetics of the isothermal (pearlite) decomposition of austenite in steel containing 0.4% C and 8.5% Cr (a 50% transformation). 1 – experimental; 2 – calculated as controlled by the $\gamma \rightarrow \alpha$ iron lattice transformation; 3 – calculated as controlled by carbon diffusion.

In chromium steel (C_0 = 8.5% Cr) the carbide $(FeCr)_7C_3$ is formed, while at lower temperatures $(FeCr)_3C$ is formed. According to reference 62, $D_{0k} = 10$ cm^2/sec and Q_k = 75 kcal/mole. At 700°, S_0 reaches 10^{-4} cm. From (111) we have

$$v < 10^{-11} \text{ cm/sec}. \qquad (112)$$

Thus the pearlite transformation in chromium steels cannot be limited by chromium diffusion, which would have made the growth rate of pearlite six to seven orders of magnitude slower than the observed rate. Carbide formation takes place in the cementite-ferrite mixture already formed. The situation seems to be similar in the case of alloying with manganese, nickel, and some other elements distinguished by large activation energies for diffusion. In some instances, however, as in alloying with Mo, the pearlite growth rate is controlled by the diffusion of the alloying element. A calculation, based on (109), of the pearlite growth rate as austenite decomposes at 675° in molybdenum steel (0.5% Mo) furnishes the result v = ~ 10^{-9} cm/sec (D_{0k} = 0.1 cm^2/sec, Q = 59 kcal/mole).[62] The experimental growth rate of pearlite for this steel is 2×10^{-6} cm/sec.[63] In the case of molybdenum steels we cannot exclude the possibility that austenite decomposes directly into ferrite and a special carbide, as has been observed experimentally.[18] However, this question requires separate study.

An analysis of the equations describing the process when limited by lattice reconstruction or by carbon diffusion shows that the kinetics of the pearlite transformation depends basically on changes of the quantities U, Q, and W in the exponential. The changed value of the difference U – Q with alloying is a criterion for determining the type of kinetics of the pearlite transformation and the possibility of describing it as limited by one or the other of the indicated mechanisms.

The curves in Fig. 27 represent the kinetics of the pearlite transformation (η = 0.5) as calculated with the $\gamma \rightarrow \alpha$ lattice transformation as the controlling process (curve 2), with carbon diffusion as the controlling process (curve 3), and according to experi-

ment.[59] In this case the pearlite transformation appears to be controlled by the lattice transformation. This confirms the opinion, agreeing with reference 61, that the kinetics of the pearlite transformation is controlled by lattice reconstruction in alloy steels, whereas carbon diffusion is the controlling process in unalloyed and low-alloy steels. An analysis of the change of the activation energy for the two mechanisms shows that in chromium steel containing more than 2.5% chromium the kinetics of the pearlite transformation is controlled by the polymorphic transformation.

A similar analysis can be carried out for steels of different composition. A consideration of the cases in which the decisive role is played by diffusion of the alloying element, leading to the formation of special carbides, requires a deeper study of the thermodynamics properties of the latter.

V. CONCLUSION AND DEDUCTIONS

The complexity and diversity of the factors affecting isothermal processes in undercooled solid solutions require that a quantitative theoretical study be based on a physically valid model of the mechanism involved. Comparison of the theoretical calculations with experiment serves to check the selected model and thus determines the most essential factors controlling the given effect while rejecting secondary factors.

The analysis of phase transformation kinetics in one-component systems leads to the conclusion that in such cases the growth rate of new-phase nuclei is controlled by the rate at which atoms surmount the potential barriers opposing their transfer to the structure of the new modification. Nuclei grow with increasing speed as they are enlarged beyond the critical size; the growth rate of sufficiently large nuclei becomes practically independent of size. This picture becomes complicated in the isothermal decomposition of solid solutions. For example, in the isothermal decomposition of austenitic carbon steel the kinetics of the process and the form of the precipitated new phase depend essentially on the initial composition of the solid solution and on the transformation temperature. In the upper subcritical region 723 — 600° C undercooled hypoeutectoid austenite precipitates spherical ferrite nuclei containing less carbon than the initial solid solution. When the nuclei are near critical size the kinetics depends on the transfer rate of iron atoms from the austenite lattice to the ferrite lattice. The process is limited by the carbon diffusion rate, beginning at a certain size limit. Nuclei considerably larger than the critical size grow at a rate inversely proportional to the square root of time. A comparison with experiment shows that the calculation conveys correctly the character of the temporal change of the nuclear growth rate, although the calculated values are smaller than the experimental values.

Nuclei appearing in the decomposition of undercooled hypoeutectoid or hypereutectoid austenite consist of a single phase, but nuclei of the eutectoid pearlite arising through the decomposition of undercooled austenite containing about 0.8% C consist of alternate ferrite and cementite lamellae. The calculated temporally constant rate at which the edges of these lamellae advance depends on temperature in the same way as the experimental result. However, although the correct order of magnitude is given for the growth rate of pearlite nuclei as compared with experimental results obtained on industrial eutectoid steels, theory and experiment disagree considerably in the case of high-purity eutectoid steel. In the latter case the calculated edgewise growth rate of a pearlite grain is 10 — 15 times smaller than the experimental rate.

Some accelerating factor has obviously been omitted from the foregoing model, just as in the case of the growth of ferrite nuclei. S. T. Konobeevskii has pointed out that this factor lies in the stresses resulting from the transformation, which impart an autocatalytic character to the process. The nuclear growth rate taking these stresses into account approaches the experimental result much more closely. The foregoing calculation of the stress field around a nucleus indicates the regions, located at phase interfaces, in which plastic deformation can occur. The questions regarding the calculation of transformation-induced stresses are intimately related to the problem of alloy hardening through dispersive precipitation of the new phase.[64]

In ternary systems the third element can produce considerable change in the aforementioned nuclear radius limit ρ_{lim}, and thus either weaken or enhance the role of the lattice reconstruction mechanism. For example, in the iron-carbon-chromium system ρ_{lim} is considerably increased by the presence of chromium, and the influence of the reconstruction mechanism is consequently strengthened. For a fixed chromium content, an increase of the carbon content accelerates the process by changing the relationship between the factors affecting the kinetics. Finally, in the pearlite transformation the addition of chromium makes the reconstruction mechanism dominant.

The foregoing theoretical treatment must be expanded to include a large number of different systems and to refine the different thermodynamic and kinetic parameters of the pertinent processes. Interaction between new-phase nuclei must also be taken into account in later stages. It is extremely important to extend the theory to cover nonisothermal processes.

The parts played by different kinds of defects, such as dislocations, grain boundaries, vacancy clusters etc., have become increasingly clear in recent years. For example, the acceleration of diffusion processes at the grain boundaries of polycrystalline alloys makes a solid solution decompose predominantly in these regions; during the tempering of steel, carbides can precipitate directly at dislocations; microcavities influence the kinetics of graphitization in cast iron etc. These effects can be important, especially in the decomposi-

tion of solid solutions at relatively low temperatures. However, the study of the decomposition kinetics of solid solutions taking inhomogeneities of the initial medium into account is still hampered by a lack of reliable experimental data, or even of clear theoretical concepts, although individual attempts have been made to take such factors into account. The science of metals and alloys is being directed generally toward this type of study. Investigators are especially interested in the influences exerted by different structural and concentrational inhomogeneities on the properties and course of processes in metals and alloys. The neglect of defects in the present review article is a simplifying assumption, which in some instances can affect the results obtained from a theoretical description of the decomposition of supersaturated solid solutions in real metals and alloys. Our analysis has shown, however, that the approximation can lead to a satisfactory explanation of some characteristics of the processes under investigation.

[1] Проблемы металловедения и физ. металлов (Problems of Metallography and the Physics of Metals), Metallurgizdat, Moscow, collections for 1949, 1951, 1952, 1955, and 1958.

[2] S. S. Shteĭnberg, Металловедение (Metallography), Vol. I, Metallurgizdat, Moscow, 1952.

[3] Ya. I. Frenkel', Кинетическая теория жидкостей (Kinetic Theory of Liquids), AN SSSR, 1945.

[4] Ya. B. Zel'dovich, JETP **12**, 526 (1942).

[5] B. Ya. Lyubov and A. L. Roĭtburd, op. cit. ref. 1, **5**, 91 (1958).

[6] Ya. I. Frenkel', JETP **9**, 952 (1939).

[7] B. Ya. Lyubov and A. L. Roĭtburd, DAN SSSR **111**, 630 (1956).

[8] D. Turnbull and J. C. Fisher, J. Chem. Phys. **17**, 71 (1949).

[9] B. Ya. Lyubov, DAN SSSR **72**, 273 (1950).

[10] B. Ya. Lyubov, op. cit. ref. 1, **5**, 294 (1958).

[11] A. N. Kolmogorov, Izv. AN SSSR Ser. Fiz. No. 3, 365 (1937).

[12] B. Ya. Pines, JETP **18**, 29 (1948).

[13] B. Ya. Pines, JETP **18**, 831 (1948).

[14] C. Zener, J. Appl. Phys. **20**, 950 (1949).

[15] C. Zener, Trans. AIME **167**, 513 and 550 (1946), Abstracts in Metals Technology No. 1 (1946).

[16] M. C. Smith, Alloy Series in Physical Metallurgy, Harper, New York, 1956.

[17] Petrova, Lapshina, and Shvartsman, DAN SSSR **121**, 1021 (1958), Soviet Phys.-Doklady **3**, 872 (1959).

[18] R. I. Entin, Превращения аустенита в стали (Austenite Transformations in Steel), Metallurgizdat, Moscow, 1960.

[19] I. M. Lifshitz and V. V. Slezov, JETP **35**, 479 (1958), Soviet Phys. JETP **8**, 331 (1959).

[20] I. M. Lifshitz and V. V. Slezov, Физ. твердого тела **1**, 1401 (1959), Soviet Phys.-Solid State **1**, 1285 (1960).

[21] N. S. Fastov, Физ. мет. и металловед (Phys. of Metals and Metallography) **7**, 354 (1959).

[22] B. Ya. Lyubov, Trudy, Scientific and Technical Soc. for Ferrous Metals **3**, 39 (1955).

[23] B. Ya. Lyubov, DAN SSSR **60**, 795 (1948).

[24] B. Ya. Lyubov, op. cit. ref. 1, **1**, 316 (1949).

[25] M. E. Blanter, Заводск. лаборатория (Plant Laboratory) No. 3 (1948).

[26] V. E. Neĭmark and I. B. Piletskaya, op. cit. ref. 1, **3**, 376 (1952).

[27] A. A. Bochvar, Исследование механизма и кинетики кристаллизации сплавов эвтектического типа (An Investigation of the Mechanism and Kinetics of Eutectic Alloy Crystallization), Gostekhizdat, Moscow, 1935.

[28] L. N. Aleksandrov, Изв. вузов (Физика) (News of the Colleges—Physics) No. 4, 102 (1961).

[29] M. P. Arbuzov, Вопросы физ. металлов и металловедения (Problems in the Physics of Metals and Metallography), Kiev, Coll. No. 6, 26 (1955).

[30] B. Ya. Lyubov and A. L. Roĭtburd, DAN SSSR **131**, 809 (1960), Soviet Phys.-Doklady **5**, 345 (1960).

[31] J. C. Fisher, Trans. AIME **185**, 688 (1949) [J. Metals **1**, (1949)].

[32] W. A. Brandt, J. Appl. Phys. **16**, 139 (1945).

[33] B. Ya. Lyubov, J. Tech. Phys. (U.S.S.R.) **20**, 872 (1950).

[34] A. I. Gardin and A. P. Gulyaev, ibid. **23**, 2001 (1953).

[35] I. L. Mirkin, Trans. MIS (Oborongiz) **18** (1941).

[36] Hull, Colton, and Mehl, Trans. AIME **150**, 185 (1942).

[37] W. S. Gorsky, Physik. Z. Sowjetunion **8**, 457 (1935).

[38] S. T. Konobeevskii, JETP **13**, 200 (1943).

[39] S. T. Konobeevskii, JETP **13**, 418 (1943).

[40] M. I. Zakharova and N. F. Lashko, Izv. AN SSSR, Ser. Tekh. No. 7, 1015 (1946).

[41] B. Ya. Lyubov and N. S. Fastov, DAN SSSR **84**, 939 (1952).

[42] N. N. Lebedev, Температурные напряжения в теории упругости (Thermal Stresses in the Theory of Elasticity), Gostekhizdat, Moscow, 1937.

[43] B. Ya. Lyubov, J. Tech. Phys. (U.S.S.R.) **20**, 1344 (1950).

[44] V. V. Sokolovskii, Теория пластичности (Theory of Plasticity), Moscow, 1950).

[45] A. H. Cottrell, Dislocations and Plastic Flow in Crystals, Oxford, 1953.

[46] L. N. Aleksandrov and B. Ya. Lyubov, DAN SSSR **74**, 1081 (1950).

[47] L. N. Aleksandrov and B. Ya. Lyubov, loc. cit. ref. 1, **2**, 256 (1951).

[48] L. N. Aleksandrov, Dopovidi (Trans.) AN Ukr. SSR No. 5, 337 (1953).

[49] L. N. Aleksandrov and B. Ya. Lyubov, loc. cit. ref. 1, **5**, 317 (1958)

[50] I. S. Gaev and V. V. Polovnikov, J. Tech. Phys. (U.S.S.R.) **25**, 529 (1955).

[51] N. F. Bolkhovitinov, Металловедение и термическая обработка (Metallography and Heat Treatment),

Mashgiz, Moscow, 1958.

[52] L. N. Aleksandrov and B. Ya. Lyubov, op. cit. ref. 21, **8**, 216 (1959).

[53] Gruzin, Kornev, and Kurdyumov, DAN SSSR **80**, 49 (1951).

[54] R. F. Mehl and U. K. Hagel, Успехи физ. металлов (Progress in Metal Physics) **3**, 88 (1960).

[55] Frye, Stansburg, and McElroy, Trans. AIME **197**, 219 (1953).

[56] E. C. Bain, Functions of the Alloying Elements in Steel, Am. Soc. for Metals, 1939.

[57] P. L. Gruzin, DAN SSSR **100**, 65 (1955).

[58] R. I. Entin, loc. cit. ref. 1, **1**, 275 (1949).

[59] L. I. Kogan and R. I. Entin, loc. cit. ref. 1, **2**, 204 (1951).

[60] L. N. Aleksandrov, op. cit. ref. 21, **7**, 169 (1959).

[61] R. I. Entin, loc. cit. ref. 1, **3**, 105 (1952).

[62] Umanskii, Finkel'shtein, Blanter, Kishkin, Fastov, and Gorelik, Физическое металловедение (Physical Metallography), Metallurgizdat, Moscow, 1955.

[63] R. W. Parcell and R. F. Mehl, Trans. AIME **194**, 771 (1952).

[64] Структура и свойства металлов и сплавов (Structure and Properties of Metals and Alloys), Metallurgizdat, Moscow, 1958.

[65] B. Ya. Pines, J. Tech. Phys. (U.S.S.R.) **24**, 1521 (1954).

Translated by I. Emin